2024 IEEE/ASME International Conference on Advanced Intelligent Mechatronics (AIM)
July 15-19, 2024. Boston, MA, USA

# Add-On Fluidic Control System for Enhancing Intraocular Pressure Stabilization and Reducing Tissue Deformation

Yu-Ting Lai[1], Aya Barzelay[2], and Tsu-Chin Tsao[1]

***Abstract*— Maintaining introaocular pressure stability is critical to surgical effectiveness and safety in intraocular surgery. In cataract lens removal procedure, the continuous fluid irrigation and aspiration creates disturbances in the intraocular pressure, which subsequently causes deformation and damage to intraocular tissues. Incidental surge phenomena, when materials blocking the aspiration pathway are suddenly released, creating sudden pressure drop and cornea collapse. To improve the pressure stability under such severe pressure disturbances, this paper presents an add-on irrigation and pressure control system to existing fluid control machine. The effect of the enhanced dynamic response for the closed loop pressure control is demonstrated by reduced corneal deformation in pig eye experiment.**

## I. Introduction

Cataract causes 45% of blindness worldwide [1] and is one of the most frequently performed surgery with over 20 million operations that were carried out annually [2]. Standard operation includes breaking up the hardened lens material, removing the lens with strong aspiration, and injecting the intraocular lens [3]. To increase surgical safety, irrigation with viscosurgical devices were used to compensate for the strong aspiration [4], however, adequate fluidics control is necessary to avoid large intraocular pressure (IOP) fluctuations. Higher IOP will enlarge the anterior chamber, stretching the cornea and iris, and causing pain in human patients [5]. On the other hand, lower IOP will decrease the gap between the surgical tool and intraocular tissues when performing the surgery, causing tissue damages and further complications [6]. To this date, foot pedal is still being used by the surgeons to control the aspiration, which further introduces uncertainties in controlling the surgical environment.

Even though the surgeons are professionally trained to accurately control the foot pedal and and reach stable environment, involuntary surge still occurs during the cataract extraction (Fig. 1) [7]. Surge phenomenon is categorized into four stages. In the first stage the surgical tool is performing normal aspiration for the cataract lens removal, where large pieces of lens materials are expected to ”come” to the aspiration port, causing partial occlusion. Full occlusion occurs at the second stage when the aspiration port is not large enough to accommodate the piece all at once, where the aspiration is not physically engaged in the anterior chamber and builds up the IOP. During stage three, the occlusion will eventually break and the aspiration force is suddenly engaged, lowering the IOP, thereby simultaneously creating the collapse of the anterior chamber. This stage is also referred to as the surge due to the sudden IOP drop, increasing the chance of tissue damage. At final stage, the provided irrigation will gradually recover the IOP back to its natural level. Therefore, the response of irrigation determines the surge level and it is desirable to avoid surge phenomenon during the surgery to increase the surgical outcome without any tissue damage.

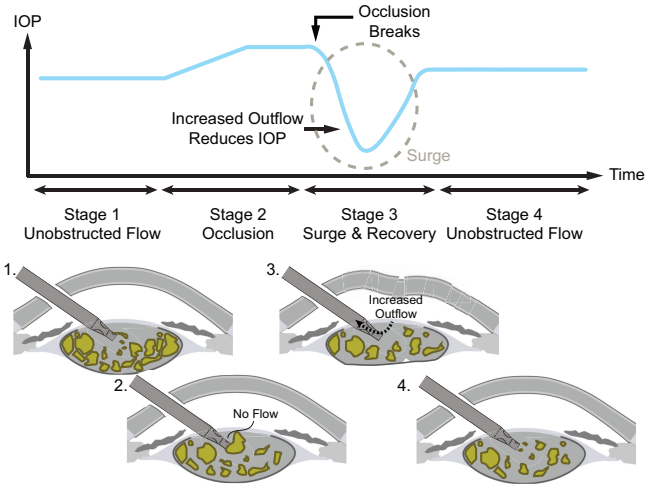


Fig. 1. The illustration of surge phenomenon due to occlusion at the aspiration port.

Commercially available fluid control machines such as the Constellation Vision Systems (Alcon Laboratories, Inc) has provided a pressure regulation algorithm to avoid surge based on irrigation flow rate measurements and aspiration flow rate inference [8]. However, the application of such method is surgery-specific and is only limited to vitreoretinal surgeries [9], thus not applicable to cataract-related procedures. Moreover, the IOP regulation performance have a slow settling time and a bias in steady-state [10], which is considered undesirable for surgical practice. Several other fluid control systems such as Stellaris (Bausch and Lomb, Vaughan, Ontario, Canada) and EVA Phaco-vitrectomy System (D.O.R.C. International, Zuidland, The Netherlands) are also widely used in clinics with fast irrigation and aspiration capabilities, but these systems possess large IOP fluctuation [11] and still have slow response time against large aspiration disturbances [12]. As a result, a faster irrigation system and control algorithm are required to increase the dynamic responses for surge avoidance.

The main scope of this work is to address the problems and develop an irrigation system based on an existing fluid control machine. We identified the technical challenges presented in cataract lens extraction, and converted the surgical requirements to technical requirements for real-time fluidics

TABLE I

ABBREVIATIONS AND DEFINITIONS USED IN THIS PAPER

| Abbreviation | Definition | Explanation |
|---|---|---|
| PC | Posterior Capsule | The thin, transparent membrane at the back of the eye lens |
| PCR | Posterior Capsule Rupture | Breakage of the PC –a serious surgical complication |
| IOP | Intraocular Pressure | Pressure inside the anterior chamber |
| OCT | Optical Coherence Tomography | A noninvasive imaging modality utilizing low-coherence interferometry. |
| IV pole | Intravenous pole | A device that holds a bag of solution and minister fluid through a tube |

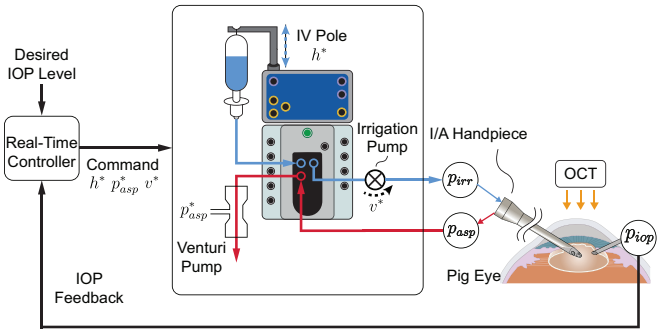


Fig. 2. The fluidic system with the add-on irrigation pump, pressure sensors and controller to the existing commercial unit. The OCT is placed above the pig eye to monitor the tissue positions.

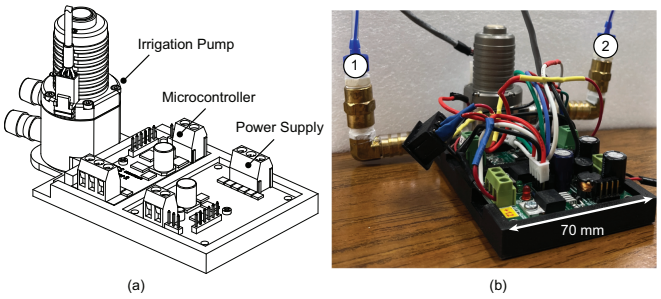


Fig. 3. Developed add-on fluid system (a) CAD model with the irrigation pump, microcontroller, and power supply. (b) Physical pump system. Note: Labeled number 1 is connected to the fluid control machine and number 2 is connected to the surgical instrument.

control. Specifically, this paper focuses on the following: (a) Development of an independent and fast irrigation system that can be attached to existing fluid control machines, (b) Development of an accurate pressure regulation strategy to compensate for surge phenomenon and increase surgical safety, and (c) Evaluation of reduced anterior chamber collapse through an optical coherence tomography (OCT) system.

The rest of this paper is organized as follows. The system overview and hardware design is introduced in Section II, followed by the fluidics modeling in Section III. Section IV shows the effectiveness of fast IOP irrigation control with OCT evaluation. Finally, Section V concludes this article. The abbreviations used throughout the article are summarized in Table I.

## II. SYSTEM AND HARDWARE DESIGN

### A. System Architecture

The system architecture is shown in Fig. 2. A straight irrigation/aspiration (I/A) handpiece with a side aspiration port (8172 UltraFLOW; Alcon Laboratories, Inc) was integrated in the system because it is commonly used for cataract lens removal [13], [14]. The rear aspiration port of the I/A handpiece was directly connected to a fluid control machine (Stellaris Elite, Bausch and Lomb, Laval, Quebec, Canada) to provide computer-controlled aspiration ($p^*_{asp}$). The rear irrigation port of the I/A handpiece was connected to an inline irrigation pump (Model M510S-180-V; TCS Micropumps, Highfield, UK). The irrigation pump was powered by a 5 V power supply with adjustable voltage command ($v^*$). The other port of the irrigation pump was connected to a bottle filled with balance salt solution (BSS) with its fluid level set by the intravenous (IV) pole above the tip of the I/A handpiece ($h^*$). The pump creates unobstructive flow when the voltage command is set to 0 V, and additional flow rates with nonzero voltage command, which subsequently changes the IOP. This forms a dual-stage irrigation system where the fluid connections with the fluid control machine and the I/A handpiece is shown in Fig. 3.

Two inline pressure sensors (24PCCFG6G, Honeywell International Inc., Charlotte, NC, USA) were embedded in the connections 2 and 3 in Fig. 3 to measure the pressure of the irrigation and aspiration pressure ($p_{irr}$ and $p_{asp}$ from the I/A handpiece without interfering the fluidics. A PCB-mounted pressure sensor (ABPDANT015PGAA5, Honeywell International Inc., Charlotte, NC, USA) was used to directly measure the IOP ($p_{iop}$). Calibration of each sensor was performed with different fluid levels and the output voltages were converted to physical pressure unit as mmHg.

An optical coherence tomography (OCT) system (Telesto II 1060LR with objective lens LSM04BB; ThorLabs) with a 1060 nm central wavelength was integrated into the system and the probe was mounted on top of the eye. A B-scan from the OCT provides a cross-sectional view of the eye anatomy and was used to monitor intraocular tissues during the whole procedure. The axial resolution of the OCT is 9.18 µm, lateral resolution is 25 µm, with a B-scan acquisition rate of approximately 10 Hz.

## III. MODEL-BASED CONTROLLER DESIGN

During cataract lens removal, large aspiration force (400 to 600 mmHg) is required to efficiently remove the cataract lens materials [15]. Such a large aspiration force has a high correlation between surgical complications such as

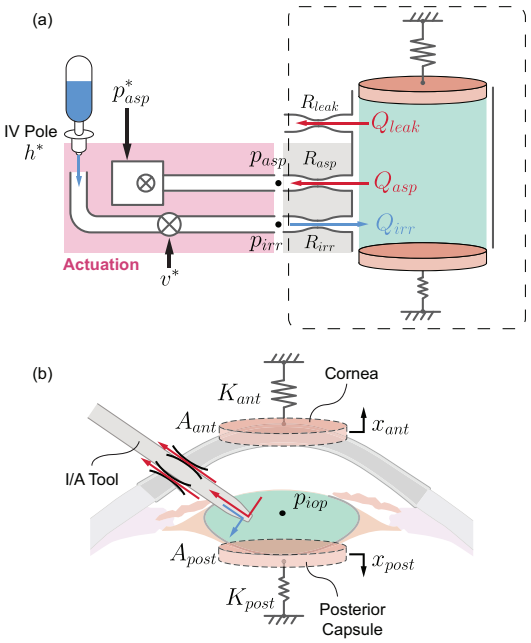


Fig. 4. Illustration of the eye anatomy and physical variables used in this paper. (a) Overall diagram with fluid actuation, surgical instrument, and the anterior chamber. (b) The zoom in view of the anterior chamber in (a) that includes the modeling of the anterior chamber.

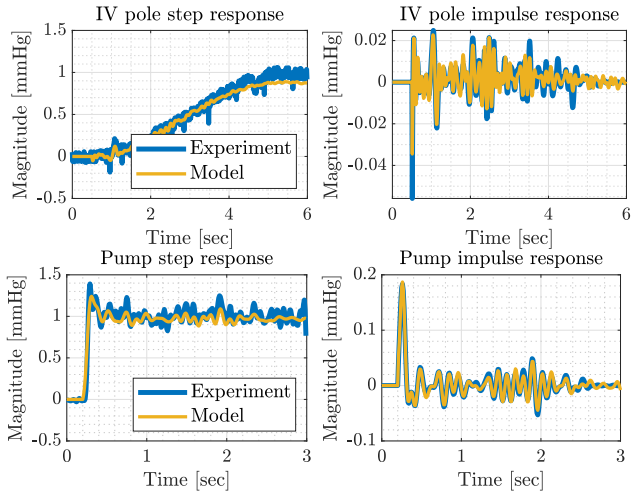


Fig. 5. The step and impulse dynamics between the experiment and identified dynamics for (a) IV pole. (b) Irrigation pump.

glaucoma [16]. In order to maintain the efficiency of lens removal while avoiding causing surgical complications, the developed controller utilizes the irrigation pump for fast IOP regulation and increases the safety of cataract surgery. To facilitate the design of the irrigation controller, a bio-mechanical model was constructed (Fig. 4), where the fluid actuation, fluid paths in an I/A handpiece, and the simplified mechanical model of the anterior chamber were depicted. These components were cascaded serially and formed the open-loop model of the system.

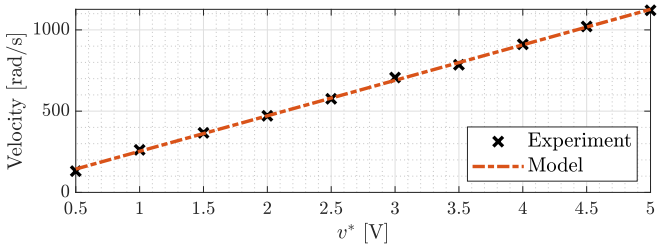


Fig. 6. The relationship between input voltage and the resultant angular velocity for pump modeling.

### A. *Fluid Transmission Dynamics*

The dynamics of the irrigation fluid transmission was first identified, where the resultant irrigation pressure $p_{irr}$ can be measured from the pressure sensor. The IV pole has a maximum stroke of 950 mm and the irrigation pump has a maximum voltage at 5V. The IV pole dynamics describes the position command $h^*$ of the IV pole to the measured $p_{irr}$, and the pump dynamics shows the voltage command $v^*$ to the output $p_{irr}$. The procedure was done using a step input command of each actuator and the resultant normalized irrigation step response is shown in Fig. 5. As can be seen, the IV pole contains a slow dynamics with a 0.5 s delay and a slew rate of approximately 16 mmHg/s, whereas a transmission delay of 0.2 s and a rise time of approximately 0.6 s were observed in the pump dynamics that is superior to the IV pole dynamics. A 30th-order and 25th-order state-space models (Eq. 1) were realized using Ho-Kalman method to adequately capture higher-order dynamics of both actuators.

$$\begin{aligned} x(k+1) &= Ax(k) + Bu(k) \\ y(k) &= Cx(k) + Du(k) \end{aligned} \tag{1}$$

Since the pump converts electrical energy to mechanical energy, this in turn linearly increases the flow rates of the irrigation line. According to Hagen–Poiseuille equation for incompressible fluid, the pressure change $\Delta p$ can be described as:

$$\Delta p = \frac{1}{2}\rho(\frac{Q}{\pi r^2})^2 \tag{2}$$

, where $\rho$ is the fluid density, r is the pipe radius, and Q is the volumetric flow rate of the pipe. Therefore, it is required to identify the linear relationship between flow rate and the input voltage. Ten different voltage commands $v^*$ were applied to the pump and the angular velocity was obtained by measuring the pulse frequencies with an oscilloscope. As indicated in Fig. 6, the input voltage to output angular velocity is linear and includes a deadzone from 0 to 0.3 V. This angular velocity was subsequently correlate with the pressure change ($\Delta p_{irr}$) from the experimental data. These identified actuator dynamics are then used for the modeling of the bio-mechanical system.

### B. Bio-mechanical Model

The anterior chamber was modeled as a closed chamber and the fluidics was described with three fluid paths: (1) $Q_{leak}$, leakage flowing out of the anterior chamber through corneal incision to the atmosphere ($p_{atm} = 0$), (2) $Q_{asp}$, outflow from the anterior chamber to the I/A handpiece due to the aspiration force ($p_{asp}$), (3) $Q_{irr}$, inflow from the I/A handpiece to the anterior chamber results from the IV pole and irrgation pump ($p_{irr}$). The fluid dynamics from these determines the IOP ($p_{iop}$) and the pressure difference can be calculated with resistive elements $R_{leak}$, $R_{asp}$, and $R_{irr}$ through Hagen–Poiseuille equations:

$$R_{leak}Q_{leak} = p_{iop} \tag{3}$$
$$R_{asp}Q_{asp} = p_{iop} - p_{asp} \tag{4}$$
$$R_{irr}Q_{irr} = p_{irr} - p_{iop} \tag{5}$$

The resistive values can be computed from the known geometry of the I/A handpiece using Equation (6) [17], and the pressures can be measured from the pressure sensors.

$$R = \frac{8\eta L}{\pi r^2} \tag{6}$$

In this equation, $\eta$ is the flow viscosity and $L$ is the length of the tube. The lumped resistance for $R_{leak}$, $R_{asp}$, and $R_{irr}$ are reported in Table II.

TABLE II
IDENTIFIED RESISTIVE PARAMETERS

| Resistive Parameter | $R_{leak}$ | $R_{asp}$ | $R_{irr}$ |
|---|---|---|---|
| Value | $9.7 \times 10^{10}$ | $7.5 \times 10^{11}$ | $5.1 \times 10^{14}$ |

Two mechanical pistons were used to describe the effect of IOP onto the cornea and posterior capsule (PC). These two tissues are parameterized with a cornea stiffness $K_{ant}$ and PC stiffness $K_{post}$, and their locations ($x_{ant}$ and $x_{post}$) can be represented by force balance equations:

$$K_{ant}\left(x_{ant} - x^0_{ant}\right) = A_{ant}p_{iop} \tag{7}$$
$$K_{post}\left(x_{post} - x^0_{post}\right) = A_{post}p_{iop} \tag{8}$$

where $x^0_{(\cdot)}$ are tissue positions in their natural shapes, and $A_{ant}$ and $A_{post}$ are effective areas of the cornea and PC surface.

Combined with fluid continuity equation, the lumped system can be represented as a single-input-single-output system with $p_{iop}$ as the state variable:

$$\underbrace{\dot{p}_{iop}}_{\dot{x}} = \underbrace{\frac{(R^{-1}_{irr} - R^{-1}_{leak} - R^{-1}_{asp})}{(\theta_{cornea} + \theta_{pc})}}_{A}\underbrace{p_{iop}}_{x} + \underbrace{\frac{R^{-1}_{irr}}{(\theta_{cornea} + \theta_{pc})}}_{B}\underbrace{p_{irr}}_{u} + \underbrace{\frac{R^{-1}_{asp}}{(\theta_{cornea} + \theta_{pc})}}_{F}\underbrace{p_{asp}}_{w} \tag{9}$$

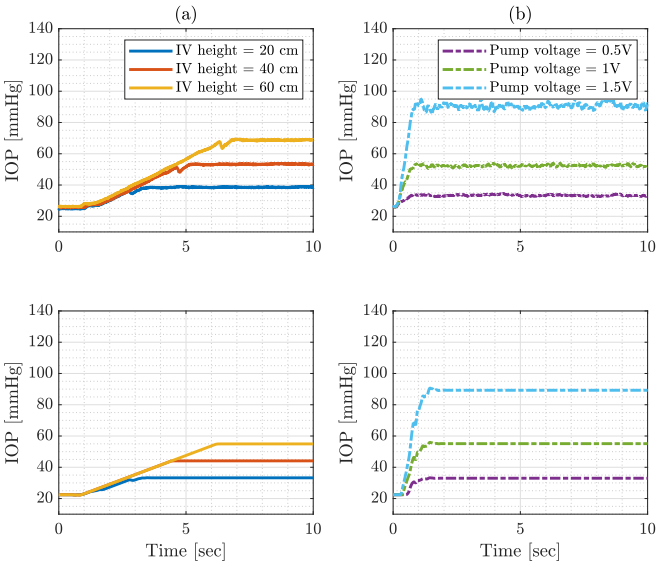


Fig. 7. Open loop IOP response under different step commands. (a) IV pole height ($h^*$). (b) Irrigation pump voltage ($v^*$). First row: experiment with *ex-vivo* pig eye verification. Second row: simulation model.

where $\theta_{cornea} = A^2_{ant}/K_{ant}$ and $\theta_{pc} = A^2_{post}/K_{post}$. Taking the Laplace transform, we can represent the dynamics as

$$P_{iop} = G_{irr}P_{irr} + G_{asp}P_{asp} \tag{10}$$

with $G_{asp}$ and $G_{irr}$ represented the pressure transmissions $\frac{P_{iop}}{P_{asp}}$ and $\frac{P_{iop}}{P_{irr}}$

$$G_{irr} = [(\theta_{ant} + \theta_{post})R_{irr}s + (1 - \frac{R_{irr}}{R_{leak}} - \frac{R_{irr}}{R_{asp}})]^{-1}$$
$$G_{asp} = -[(\theta_{ant} + \theta_{post})R_{asp}s + (\frac{R_{asp}}{R_{irr}} - \frac{R_{asp}}{R_{leak}} - 1)]^{-1} \tag{11}$$

The term associated with the resistive elements can be determined from previously identified values. In static transmission ($s = 0$), that term in $G_{irr}$ is positive, which means applying irrigation increases IOP. On the other hand, the negative sign in $G_{asp}$ results in IOP drop when applying aspiration.

### C. Open-Loop Response

To validate the constructed bio-mechanical model, open-loop responses between simulation and experiment were compared in Fig. 7. Different step commands ($h^*$ and $v^*$) were applied at $t = 0$ s and resultant IOP ($p_{iop}$) was recorded. Similar exponential growth trends, order of magnitude, and rise time were observed for both stages, however, the maximum change in IOP deviates from the experimental results by approximately 20% in steady-state for the IV pole.

## IV. EXPERIMENTAL RESULTS

### A. Setup and Alignment

Unscalded *ex-vivo* pig eyes were used as the eye phantom (Sioux-Preme Packing) for the experiments. The eyes were placed and were secured by pinning their excessive flesh on a

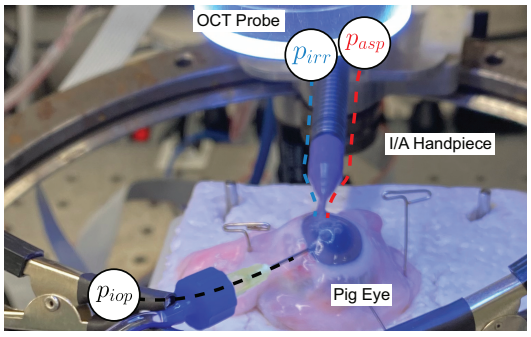


Fig. 8. Pig eye experimental setup.

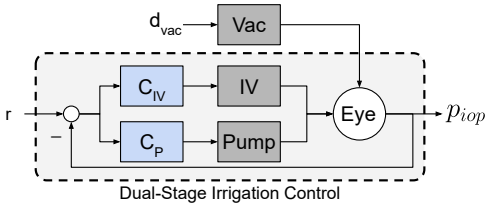


Fig. 9. Dual-stage control structure for the irrigation system where $d_{vac}$ represents the aspiration disturbance during lens extraction.

customized polystyrene holder. The preparation of each eye was performed under a surgical microscope (Opmi Lumera 700, Carl Zeiss AG). A standard corneal incision was created with a 3-mm keratome knife, followed by a 6 mm diameter continuous curvilinear capsulorhexis. Hydrodissection was performed using BSS (NDC 0065-0800-50; Alcon) to mobilize the lens materials and manual lens removal was done using a sterilized syringe.

Following eye preparation, the I/A handpiece was inserted into the pig eye from the corneal incisin such that it is approximately 4 mm inside eye. The IV pole was adjusted to be 30 mmHg [18], which introduces irrigation into the anterior chamber with the tissues remain at their natural shape during cataract surgery. The IOP pressure sensor was engaged from a secondary incision approximately 120° apart from the corneal incision and provide IOP measurements to the controller.

### B. Dual-Stage Controller Design

The control diagram of the dual-stage irrigation system is shown in Fig. 9, where $C_{IV}$ is the existing control on the IV pole and $C_P$ is the additional irrigation pump controller. A model-based proportional-integral (PI) controller was designed and realized for the irrigation pump. The PI gains were tuned based on standard Ziegler-Nichols method in the structed bio-mechanical model with a sampling rate of 100 Hz. The resultant $C_P$, along with $C_{IV}$, are as follows:

$$C_P(z) = 0.01 + \frac{0.03}{z-1} \tag{12}$$

$$C_{IV}(z) = 0.8 + \frac{0.008}{z-1} \tag{13}$$

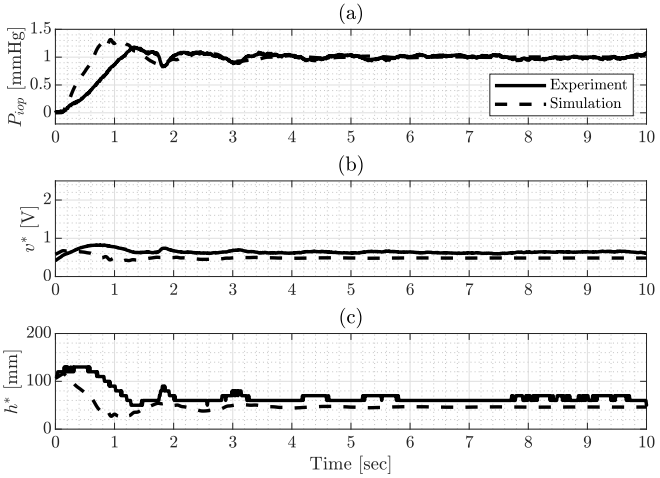


Fig. 10. Closed-loop response verification between simulation and experiment. (a) Closed-loop IOP response. (b) Pump voltage command. (c) IV pole height command.

with a gain margin of 46 dB and a phase margin of 89.7° for $C_P$, and a gain margin of 10.5 dB and a phase margin of 163° for $C_{IV}$. These are sufficiently large enough to account for model differences between each eye and ensure robustness against unmodeled dynamics and disturbances. The step responses from the simulation and pig eye experiment are compared to verify the closed-loop controller design (Fig. 10). The initial condition was set such that the IOP started at the same level and the output $p_{iop}$ is normalized to represent standard step response. The closed-loop response in the pig eye shows a rise time of approximately 0.8 s, settling time of 2 s, overshoot about 17%, and zero steady-state error. The simulation presents similar dynamics but approximately 40% faster response. The major variation between the two is due to the variation of the physical parameters where each eye contains different stiffnesses and areas.

### C. Tissue Protection

To simulate occlusion at the aspiration port, the aspiration tube was manually squeezed to limit the flow rate until full blockage was created, followed by releasing the tube to suddenly increase aspiration flow rate. This will suddenly decrease the IOP and shallows the anterior chamber, thereby providing a good example for surge experiments. To focus on the effectiveness of surge avoidance and eliminate the transient response, a strong vacuum of 600 mmHg was used and IOP control was turned on before applying the blockage. As can be seen in Fig. 11, there is an transient increase in IOP when the aspiration tube is blocked. The blockage was released at $t = 2$ s, which can be observed by the spike in $p_{asp}$ and the aspiration was suddenly engaged. IOP regulation error against this surge phenomenon is reported in Table III, where the IOP variation and root-mean-square error are largely reduced with the developed dual-stage irrigation system. In addition, tissue positions were evaluated with the OCT when the lowest IOP occurs (Fig. 12), which further showcases that the dual-stage irrigation system can avoid the

TABLE III

REGULATION ERROR AGAINST SURGE

| Error Type | RMS [mmHg] | Peak to peak [mmHg] |
|---|---|---|
| IV control only | 1.65 | 10.16 |
| Dual-stage | 0.83 | 4.63 |

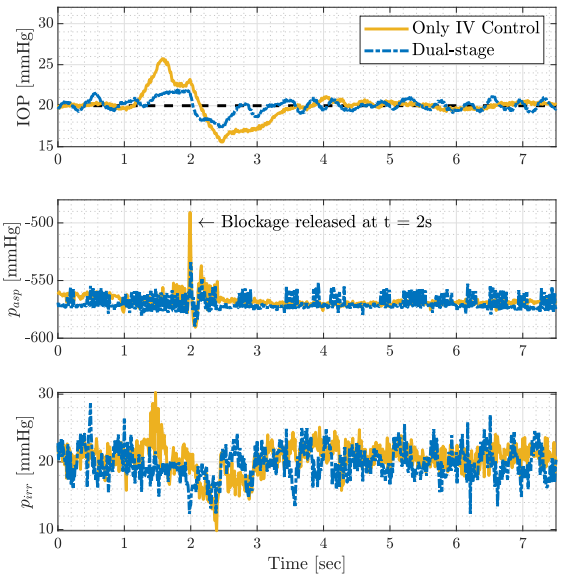


Fig. 11. Surge avoidance with IOP control.

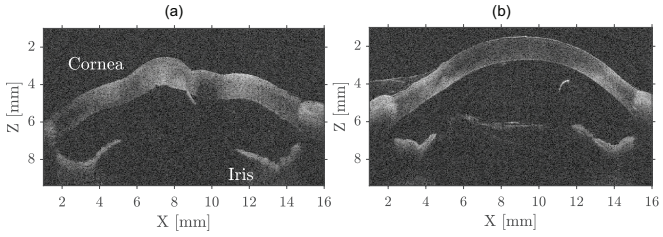


Fig. 12. OCT cross-sectional view at the lowest IOP when surge occurs with (a) IV control only and (b) dual-stage irrigation control.

deformation of the cornea and iris and reduce possible tissue damage.

## V. CONCLUSION

This paper presents an innovative strategy by integrating an add-on irrigation pump into an existing fluid control machine that increases the dynamics of pressure regulation. A bio-mechanical model was constructed for the dual-stage system and a model-based controller was designed. The capability of regulating the IOP and avoid surge phenomenon was demonstrated on *ex-vivo* pig eyes with manual aspiration tube occlusion. The experiments were conducted with OCT to monitor intraocular structures, where tissue damage was successfully avoided with the developed system and IOP control algorithm.

## REFERENCES


[1] R. Bourne, J. D. Steinmetz, S. Flaxman, P. S. Briant, H. R. Taylor, S. Resnikoff, R. J. Casson, A. Abdoli, E. Abu-Gharbieh, A. Afshin *et al.*, "Trends in prevalence of blindness and distance and near vision impairment over 30 years: an analysis for the global burden of disease study," *The Lancet global health*, vol. 9, no. 2, pp. e130–e143, 2021.

[2] A. Grzybowski and P. Kanclerz, "Recent developments in cataract surgery," *Current concepts in ophthalmology*, pp. 55–97, 2020.

[3] G. Davis, "The evolution of cataract surgery," *Missouri medicine*, vol. 113, no. 1, p. 58, 2016.

[4] M. S. Malvankar-Mehta, A. Fu, Y. Subramanian, and C. Hutnik, "Impact of ophthalmic viscosurgical devices in cataract surgery," *Journal of ophthalmology*, vol. 2020, 2020.

[5] Y. Zhao, X. Li, A. Tao, J. Wang, and F. Lu, "Intraocular pressure and calculated diastolic ocular perfusion pressure during three simulated steps of phacoemulsification in vivo," *Investigative ophthalmology & visual science*, vol. 50, no. 6, pp. 2927–2931, 2009.

[6] H. Suzuki, K. Oki, T. Shiwa, H. Oharazawa, and H. Takahashi, "Effect of bottle height on the corneal endothelium during phacoemulsification," *Journal of Cataract & Refractive Surgery*, vol. 35, no. 11, pp. 2014–2017, 2009.

[7] P. Sharif-Kashani, D. Fanney, and V. Injev, "Comparison of occlusion break responses and vacuum rise times of phacoemulsification systems," *BMC ophthalmology*, vol. 14, no. 1, pp. 1–7, 2014.

[8] D. J. K. Abulon, "Vitreous flow rates through dual pneumatic cutters: effects of duty cycle and cut rate," *Clinical Ophthalmology (Auckland, NZ)*, vol. 9, p. 253, 2015.

[9] C. D. Riemann, J. Zhou, and D. C. Buboltz, "Vitreous cutter velocities: dual pneumatic drive vs. single pneumatic drive with spring return probes," *Investigative Ophthalmology & Visual Science*, vol. 52, no. 14, pp. 6132–6132, 2011.

[10] Y. Sugiura, F. Okamoto, Y. Okamoto, T. Hiraoka, and T. Oshika, "Intraocular pressure fluctuation during microincision vitrectomy with constellation vision system," *American Journal of Ophthalmology*, vol. 156, no. 5, pp. 941–947, 2013.

[11] Y. Shinkai, K. Yoneda, and C. Sotozono, "Comparison of intraocular pressure fluctuation during pars plana vitrectomy performed with various vitrectomy systems," *Investigative Ophthalmology & Visual Science*, vol. 59, no. 9, pp. 871–871, 2018.

[12] ——, "Ex vivo comparison of intraocular pressure fluctuation during pars plana vitrectomy performed using 25-and 27-gauge systems," *Ophthalmic Research*, vol. 65, no. 2, pp. 210–215, 2022.

[13] C.-W. Chen, Y.-H. Lee, M. J. Gerber, H. Cheng, Y.-C. Yang, A. Govetto, A. A. Francone, S. Soatto, W. S. Grundfest, J.-P. Hubschman *et al.*, "Intraocular robotic interventional surgical system (iriss): semi-automated oct-guided cataract removal," *The International Journal of Medical Robotics and Computer Assisted Surgery*, vol. 14, no. 6, p. e1949, 2018.

[14] J. T. Wilson, M. J. Gerber, S. W. Prince, C.-W. Chen, S. D. Schwartz, J.-P. Hubschman, and T.-C. Tsao, "Intraocular robotic interventional surgical system (iriss): Mechanical design, evaluation, and master–slave manipulation," *The International Journal of Medical Robotics and Computer Assisted Surgery*, vol. 14, no. 1, p. e1842, 2018.

[15] T. Boulter, A. Bernhisel, C. Mamalis, B. Zaugg, W. R. Barlow, R. J. Olson, and J. H. Pettey, "Phacoemulsification in review: optimization of cataract removal in an in vitro setting," *Survey of Ophthalmology*, vol. 64, no. 6, pp. 868–875, 2019.

[16] J. P. Berdahl, "Cataract surgery to lower intraocular pressure," *Middle East African journal of ophthalmology*, vol. 16, no. 3, p. 119, 2009.

[17] O. Abouali, D. Bayatpour, A. Ghaffariyeh, and G. Ahmadi, "Simulation of flow field during irrigation/aspiration in phacoemulsification using computational fluid dynamics," *Journal of Cataract & Refractive Surgery*, vol. 37, no. 8, pp. 1530–1538, 2011.

[18] A. Grinbaum, M. Blumenthal, and E. Assia, "Comparison of intraocular pressure profiles during cataract surgery by phacoemulsification and extracapsular cataract extraction," pp. 182–186, 2003.